Statistical Modelling and Experimental Verification for Wideband MIMO Mobile-to-mobile Channels in Urban Environments

Alenka G. Zajić *, Gordon L. Stüber *, Thomas G. Pratt †, and Son Nguyen §
* School of Electrical and Computer Engineering Georgia Institute of Technology, Atlanta, GA 30332 USA
†Georgia Tech Research Institute, Atlanta, GA 30332 USA
§ Army Research Laboratory, Adelphi, MA 20783 USA

***Abstract*— A three-dimensional reference model for wideband multiple-input multiple-output (MIMO) mobile-to-mobile (M-to-M) channels is reviewed. To validate the reference model, an experimental MIMO M-to-M channel-sounding campaign was conducted for M-to-M vehicular communication with vehicles travelling along surface streets of a metropolitan area. The measured data is processed and the first- and second-order channel statistics obtained from the reference model and from the empirical measurements are compared. The close agreement between the analytically and empirically obtained channel statistics confirms the utility of the proposed reference model.**

I. Introduction

Several emerging wireless communication systems such as mobile ad-hoc wireless networks, intelligent transportation systems, and relay-based cellular networks require direct transmission between mobile terminals. Such mobile-to-mobile (M-to-M) communication systems are equipped with low elevation antennas and have both the transmitter ($\mathrm{T_x}$) and receiver ($\mathrm{R_x}$) in motion. Early studies of single-input single-output (SISO) M-to-M Rayleigh fading channels are reported in [1]. They showed that the received envelope of M-to-M channels is Rayleigh faded under non-line-of-sight conditions (NLoS), but the statistical properties differ from conventional fixed-to-mobile cellular radio channels. They also proposed the reference model for two-dimensional (2-D) SISO M-to-M Rayleigh fading channels. Simulation models for 2-D SISO M-to-M channels are proposed in [2] - [4]. Channel measurements for SISO narrowband and wideband M-to-M communications are reported in [5] and [6]. The reference models for 2-D narrowband multiple-input multiple-output (MIMO) M-to-M channels are proposed in [7] and [8]. All previously reported models are two-dimensional and accurate only for certain environments, e.g., rural areas. For urban environments where the $\mathrm{T_x}$ and $\mathrm{R_x}$ antenna arrays are often located in close proximity to and lower than surrounding buildings, the tree-dimensional (3-D) models are more appropriate. Hence, we have recently proposed the 3-D reference models for *narrowband* and *wideband* MIMO M-to-M multipath fading channels [9], [10]. We have also derived the first- and second-order statistics for the proposed models [10], [11] along width simulation models [12].

This paper verifies our 3-D wideband MIMO M-to-M reference model in [10] by using MIMO M-to-M channel measurements collected from vehicles travelling along the surface streets near Georgia Tech campus. First, we review our reference model. Then, we describe the measurement campaign and the data processing techniques used to process the measured data. Finally, we compare the space-Doppler power spectral density (sD-psd), the power space-delay spectral density (psds), and the envelope level crossing rate (LCR) obtained from the reference model with those obtained from the measured data. The close agreement between the analytical and empirical curves confirms the utility of the proposed reference model.

The remainder of the paper is organized as follows. For ease of reference, Section II reviews our 3-D wideband MIMO M-to-M reference model. Section III describes the measurement campaign and the data processing techniques used to process the measured data. Section IV compares the analytical and empirical results for the sD-psd, the psds, and the LCR. Finally, Section V provides some concluding remarks.

II. A 3-D Theoretical Model for Wideband MIMO Mobile-to-Mobile Channels

This section describes our 3-D theoretical model for wideband MIMO M-to-M multipath fading channels proposed in [10]. We consider a wideband MIMO communication system with L_t transmit and L_r receive omnidirectional antenna elements. It is assumed that both the $\mathrm{T_x}$ and $\mathrm{R_x}$ are in motion and equipped with low elevation antennas. The radio propagation occurs in outdoor metropolitan environments that are characterized by 3-D non-isotropic scattering with either line-of-sight (LoS) or non-line-of-sight (NLoS) conditions between the $\mathrm{T_x}$ and $\mathrm{R_x}$. The MIMO channel can be described by an $L_r \times L_t$ matrix $\mathbf{H}(t,\tau) = [h_{ij}(t,\tau)]_{L_r \times L_t}$ of the input delay-spread functions.

0
Prepared through collaborative participation in the Collaborative Technology Alliance for Communications & Networks sponsored by the U.S. Army Research Laboratory under Cooperative Agreement DAAD19-01-2-0011. The U.S. Government is authorized to reproduce and distribute reprints for Government purposes notwithstanding any copyright notation thereon.

The 3-D reference model is derived using the 3-D geometrical "concentric-cylinders" model shown in Fig. 1.

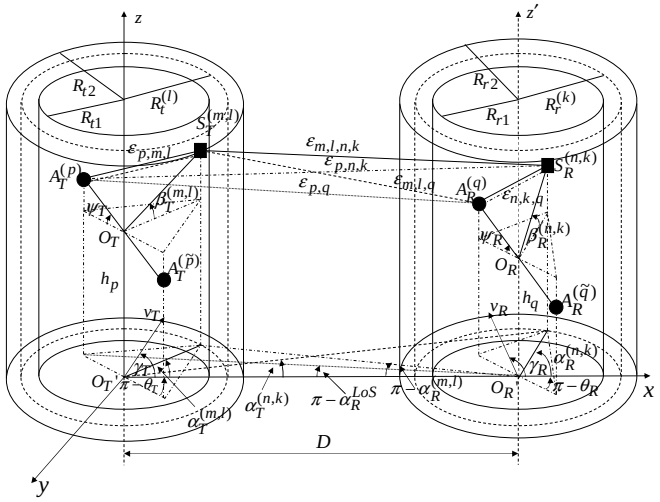

Fig. 1. The "concentric-cylinders" model with LoS, single- and double-bounced rays for a MIMO M-to-M channel with $L_t = L_r = 2$ antenna elements.

The "concentric-cylinders" model defines four cylinders, two around the $\mathrm{T_x}$ and another two around the $\mathrm{R_x}$, as shown in Fig. 1. Around the $\mathrm{T_x}$, M fixed omnidirectional scatterers occupy a volume between cylinders of radii R_{t1} and R_{t2}. It is assumed that the M scatterers lie on L cylindric surfaces of radii $R_{t1} \leq R_t^{(l)} \leq R_{t2}$, where $1 \leq l \leq L$. The l^{th} cylindric surface contains $M^{(l)}$ fixed omnidirectional scatterers, and the $(m,l)^{th}$ transmit scatterer is denoted by $S_T^{(m,l)}$. Similarly, around the $\mathrm{R_x}$, N fixed omnidirectional scatterers occupy a volume between cylinders of radii R_{r1} and R_{r2}. It is assumed that the N scatterers lie on K cylindric surfaces of radii $R_{r1} \leq R_r^{(k)} \leq R_{r2}$, where $1 \leq k \leq K$. The k^{th} cylindric surface contains $N^{(k)}$ fixed omnidirectional scatterers, and the $(n,k)^{th}$ receive scatterer is denoted by $S_R^{(n,k)}$. The parameters in Fig. 1 are defined in Table I. It is assumed that the radii R_{t2} and R_{r2} are much smaller than the distance D, i.e., $\max\{R_{t2}, R_{r2}\} \ll D$ (local scattering condition). Furthermore, it is assumed that the distance D is smaller than $4R_{t1}R_{r1}L_r/(\lambda(L_t-1)(L_r-1))$ (channel does not experience keyhole behavior [14]), where λ denotes the carrier wavelength. Finally, it is assumed that d_T and d_R are much smaller than the radii R_{t1} and R_{r1}, i.e., $\max\{d_T, d_R\} \ll \min\{R_{t1}, R_{r1}\}$.

Observe from the 3-D geometrical model that some waves from the $\mathrm{T_x}$ antenna may traverse directly to the $\mathrm{R_x}$ antenna, while others are single- and/or double-bounced before arriving at the $\mathrm{R_x}$ antenna. Hence, the time-variant transfer function (i.e., the Fourier transform of the input delay-spread function) of the link $A_T^{(p)}$ - $A_R^{(q)}$ can be written as a superposition of the LoS, single-bounced transmit, single-bounced receive and double-bounced rays [10]

$$T_{pq}(t,f) = T_{pq}^{LoS}(t,f) + T_{pq}^{SBT}(t,f) + T_{pq}^{SBR}(t,f) + T_{pq}^{DB}(t,f). \quad (1)$$

TABLE I

DEFINITION OF PARAMETERS IN FIGURE 1.

D	The distance between the centers of the Tx and Rx cylinders.
$R_t^{(l)}, R_r^{(k)}$	The radius of the l^{th} Tx and k^{th} Rx cylinder, respectively.
d_T, d_R	The spacing between two adjacent antenna elements at the Tx and Rx, respectively.
θ_T, θ_R	The orientation of the Tx and Rx antenna array in the x-y plane (relative to the x-axis), respectively.
ψ_T, ψ_R	The elevation of the Tx's and Rx's antenna array relative to the x-y plane, respectively.
v_T, v_R	The velocities of the Tx and Rx, respectively.
γ_T, γ_R	The moving directions of the Tx and Rx, respectively.
$\alpha_T^{(m,l)}, \alpha_T^{(n,k)}$	The azimuth angles of departure (AAoD) of the waves that impinge on the scatterers $S_T^{(m,l)}$ and $S_R^{(n,k)}$, respectively.
$\alpha_R^{(m,l)}, \alpha_R^{(n,k)}$	The azimuth angles of arrival (AAoA) of the waves scattered from $S_T^{(m,l)}$ and $S_R^{(n,k)}$, respectively.
α_R^{LoS}	The AAoA of the LoS paths.
$\beta_T^{(m,l)}, \beta_R^{(n,k)}$	The elevation angles of departure (EAoD) and the elevation angles of arrival (EAoA), respectively.
$\varepsilon_{p,m,l}$, $\varepsilon_{m,l,q}$, $\varepsilon_{p,n,k}$, $\varepsilon_{n,k,q}$, $\varepsilon_{m,l,n,k}$ and ε_{pq}	The distances $d\left(A_T^{(p)}, S_T^{(m,l)}\right)$, $d\left(S_T^{(m,l)}, A_R^{(q)}\right)$, $d\left(A_T^{(p)}, S_R^{(n,k)}\right)$, $d\left(S_R^{(n,k)}, A_R^{(q)}\right)$, $d\left(S_T^{(m,l)}, S_R^{(n,k)}\right)$, and $d\left(A_T^{(p)}, A_R^{(q)}\right)$, respectively.
h_p, h_q	The distances $d\left(O_T, O_T^{'}\right)$ and $d\left(O_R, O_R^{'}\right)$, respectively.

We use the time-variant transfer function instead of the input delay-spread function to simplify further analysis. The single-bounced transmit, single-bounced receive, double-bounced, and LoS components of the time-variant transfer function are, respectively,

$$T_{pq}^{SBT}(t,f) = \sqrt{\frac{\eta_T \Omega_{pq}}{K_{pq}+1}} \lim_{M\to\infty} \sum_{l=1}^{L} \sum_{m=1}^{M^{(l)}} \frac{\left(1 - \frac{\gamma}{2}\frac{R_t^{(l)}}{D}\right)}{\sqrt{M}} a_{p,m,l}^{SBT}$$
$$\times\, b_{q,m,l}^{SBT} e^{j2\pi t f_{T\max} \cos(\alpha_T^{(m,l)} - \gamma_T) \cos\beta_T^{(m,l)}}$$
$$\times\, e^{j2\pi t f_{R\max}(\Delta_T^{(l)} \sin\gamma_R \sin\alpha_T^{(m,l)} - \cos\gamma_R)\cos(\Delta_T^{(l)}\beta_T^{(m,l)} + \Delta_H/D)}$$
$$\times\, e^{-j\frac{2\pi}{c_0 \cos\beta_T^{(m,l)}} f\left[D + R_t^{(l)}(1-\cos\alpha_T^{(m,l)})\right] + j\phi_{m,l}}, \quad (2)$$

$$T_{pq}^{SBR}(t,f) = \sqrt{\frac{\eta_R \Omega_{pq}}{K_{pq}+1}} \lim_{N\to\infty} \sum_{k=1}^{K} \sum_{n=1}^{N^{(k)}} \frac{\left(1 - \frac{\gamma}{2}\frac{R_r^{(k)}}{D}\right)}{\sqrt{N}} a_{p,n,k}^{SBR}$$
$$\times\, b_{q,n,k}^{SBR} e^{j2\pi t f_{R\max} \cos(\alpha_R^{(n,k)} - \gamma_R) \cos\beta_R^{(n,k)}}$$
$$\times\, e^{j2\pi t f_{T\max}(\Delta_R^{(k)} \sin\gamma_T \sin\alpha_R^{(n,k)} + \cos\gamma_T)\cos(\Delta_R^{(k)}\beta_R^{(n,k)} - \Delta_H/D)}$$
$$\times\, e^{-j\frac{2\pi}{c_0 \cos\beta_R^{(n,k)}} f\left[D + R_r^{(k)}(1+\cos\alpha_R^{(n,k)})\right] + j\phi_{n,k}}, \quad (3)$$

$$T_{pq}^{DB}(t,f) = \sqrt{\frac{\eta_{TR} \Omega_{pq}}{K_{pq}+1}} \lim_{M,N\to\infty} \sum_{l,m=1}^{L,M^{(l)}} \sum_{k,n=1}^{K,N^{(k)}} a_{p,m,l}^{DB} b_{q,n,k}^{DB}$$
$$\times\, \frac{\left(1 - \frac{\gamma}{2}\frac{R_t^{(l)} + R_r^{(k)}}{2D}\right)}{\sqrt{MN}} e^{j2\pi t f_{T\max} \cos(\alpha_T^{(m,l)} - \gamma_T) \cos\beta_T^{(m,l)}}$$
$$\times\, e^{j2\pi t f_{R\max} \cos(\alpha_R^{(n,k)} - \gamma_R) \cos\beta_R^{(n,k)}}$$
$$\times\, e^{-j\frac{2\pi}{c_0} f\left[D + \frac{R_t^{(l)}\left(1-\cos\alpha_T^{(m,l)}\right)}{\cos\beta_T^{(m,l)}} + \frac{R_r^{(k)}\left(1+\cos\alpha_R^{(n,k)}\right)}{\cos\beta_R^{(n,k)}}\right] + j\phi_{m,l,n,k}}, \quad (4)$$

$$T_{pq}^{LoS}(t,f) = \sqrt{\frac{K_{pq}\Omega_{pq}}{1+K_{pq}}} e^{j2\pi t f_{T\max}\cos\left(\pi-\alpha_{Rq}^{LoS}-\gamma_T\right)}$$
$$\times\ e^{j2\pi t f_{R\max}\cos\left(\alpha_{Rq}^{LoS}-\gamma_R\right)} e^{-j\frac{2\pi}{c_0}f\sqrt{D^2+\Delta_H{}^2}} e^{-j\frac{2\pi}{\lambda}D} \quad (5)$$
$$\times\ e^{j\frac{2\pi}{\lambda}\left[(0.5L_t+0.5-p)d_{Tx}+(0.5L_r+0.5-q)d_R\cos\psi_R\cos(\alpha_{Rq}^{LoS}-\theta_R)\right]}.$$

In (2) – (5), K_{pq} denotes the Rice factor (ratio of LoS to scatter received power) of the subchannel $A_T^{(p)} - A_R^{(q)}$, γ is the path loss exponent, λ is the carrier wavelength, c_0 is the speed of light, $f_{T\max} = v_T/\lambda$ and $f_{R\max} = v_R/\lambda$ are the maximum Doppler frequencies associated with the $\mathrm{T_x}$ and $\mathrm{R_x}$, respectively, $\Delta_T^{(l)} = R_t^{(l)}/D$, $\Delta_R^{(k)} = R_r^{(k)}/D$, $\Delta_H = h_p - h_q$, $\Omega_{pq} = D^{-\gamma}P_{pq}\lambda^2/(4\pi)^2$, and P_{pq} is the power transmitted through the subchannel $A_T^{(p)} - A_R^{(q)}$. The parameters η_T, η_R, and η_{TR} specify how much the single- and double-bounced rays contribute in the total averaged power, i.e., these parameters satisfy $\eta_T + \eta_R + \eta_{TR} = 1$. Furthermore, the parameters p and q take values from the sets $p \in \{1,\ldots,L_t\}$ and $q \in \{1,\ldots,L_r\}$. Finally, the parameters $a_{p,m,l}^{SBT}$, $b_{q,m,l}^{SBT}$, $a_{p,n,k}^{SBR}$, $b_{q,n,k}^{SBR}$, $a_{p,m,l}^{DB}$, and $b_{q,n,k}^{DB}$ are, respectively,

$$a_{p,m,l}^{SBT} = e^{j\frac{2\pi}{\lambda}(0.5L_t+0.5-p)d_{Tx}\cos\alpha_T^{(m,l)}\cos\beta_T^{(m,l)}} \quad (6)$$
$$e^{j\frac{2\pi}{\lambda}(0.5L_t+0.5-p)\left[d_{Ty}\sin\alpha_T^{(m,l)}\cos\beta_T^{(m,l)}+d_{Tz}\sin\beta_T^{(m,l)}\right]}$$
$$b_{q,m,l}^{SBT} = e^{-j\frac{2\pi}{\lambda}(D+R_t^{(l)})} \quad (7)$$
$$e^{j\frac{2\pi}{\lambda}(0.5L_r+0.5-q)d_R\cos\psi_R\rho_R\cos(\Delta_T^{(l)}\beta_T^{(m,l)}+\Delta_H/D)}$$
$$a_{p,n,k}^{SBR} = e^{-j\frac{2\pi}{\lambda}\left(D+R_r^{(k)}\right)} \quad (8)$$
$$e^{j\frac{2\pi}{\lambda}(0.5L_t+0.5-p)d_T\cos\psi_T\rho_T\cos(\Delta_R^{(k)}\beta_R^{(n,k)}-\Delta_H/D)}$$
$$b_{q,n,k}^{SBR} = e^{j\frac{2\pi}{\lambda}(0.5L_r+0.5-q)d_{Rx}\cos\alpha_R^{(n,k)}\cos\beta_R^{(n,k)}} \quad (9)$$
$$e^{j\frac{2\pi}{\lambda}(0.5L_r+0.5-q)\left[d_{Ry}\sin\alpha_R^{(n,k)}\cos\beta_R^{(n,k)}+d_{Rz}\sin\beta_R^{(n,k)}\right]}$$
$$a_{p,m,l}^{DB} = e^{-j\frac{2\pi}{\lambda}(D/2+R_t^{(l)})}e^{j\frac{2\pi}{\lambda}(0.5L_t+0.5-p)d_{Tz}\sin\beta_T^{(m,l)}} \quad (10)$$
$$e^{j\frac{2\pi}{\lambda}(0.5L_t+0.5-p)\left[d_{Tx}\cos\alpha_T^{(m,l)}\cos\beta_T^{(m,l)}+d_{Ty}\sin\alpha_T^{(m,l)}\cos\beta_T^{(m,l)}\right]}$$
$$b_{q,n,k}^{DB} = e^{-j\frac{2\pi}{\lambda}\left(D/2+R_r^{(k)}\right)}e^{j\frac{2\pi}{\lambda}(0.5L_r+0.5-q)d_{Rz}\sin\beta_R^{(n,k)}} \quad (11)$$
$$e^{j\frac{2\pi}{\lambda}(0.5L_r+0.5-q)\left[d_{Rx}\cos\alpha_R^{(n,k)}\cos\beta_R^{(n,k)}+d_{Ry}\sin\alpha_R^{(n,k)}\cos\beta_R^{(n,k)}\right]}$$

where $d_{Tx} = d_T\cos\psi_T\cos\theta_T$, $d_{Ty} = d_T\cos\psi_T\sin\theta_T$, $d_{Tz} = d_T\sin\psi_T$, $d_{Rx} = d_R\cos\psi_R\cos\theta_R$, $d_{Ry} = d_R\cos\psi_R\sin\theta_R$, $d_{Rz} = d_R\sin\psi_R$, $\rho_R = \Delta_T^{(l)}\sin\theta_R\sin\alpha_T^{(m,l)} - \cos\theta_R$, $\rho_T = \Delta_R^{(k)}\sin\theta_T\sin\alpha_R^{(n,k)} + \cos\theta_T$.

The model in [10] assumes that the angles of departure and the angles of arrival are random variables. Furthermore, it assumes that the phases ϕ_m, ϕ_n, and ϕ_{mn} are also random variables uniformly distributed on the interval $[-\pi,\pi)$ and independent from the angles of departure and the angles of arrival. The azimuth angles of departure and arrival, $\alpha_T^{(m,l)}$ and $\alpha_R^{(n,k)}$, are characterized by the von Mises probability density function (pdf), which is defined as [15] $f(\theta) = \exp\left[k\cos(\theta-\mu)\right]/2\pi I_0(k)$, where $\theta \in [-\pi,\pi)$, $I_0(\ \cdot\ )$ is the zeroth-order modified Bessel function of the first kind, $\mu \in [-\pi,\pi)$ is the mean angle at which the scatterers are distributed in the x - y plane, and k controls the spread of scatterers around the mean. The elevation angles of departure and arrival, $\beta_T^{(m,l)}$ and $\beta_R^{(n,k)}$, are characterized by the pdf [16] $f(\varphi) = \pi\cos\left(\pi\varphi/(4\varphi_m)\right)/(4|\varphi_m|)$ for $|\ \varphi\ | \leq |\ \varphi_m\ | \leq \pi/2$ and $f(\varphi) = 0$ otherwise. The parameter φ_m is the maximum elevation angle and lies in the range $0^\circ \leq |\ \varphi_m\ | \leq 20^\circ$ [17], [10]. Finally, the radii $R_t^{(l)}$ and $R_r^{(k)}$ are characterized by the pdfs $f(R_t) = 2R_t/(R_{t2}^2 - R_{t1}^2)$ and $f(R_r) = 2R_r/(R_{r2}^2 - R_{r1}^2)$, respectively, [10].

III. Measurement Campaign Description and Data Processing

This section describes our MIMO M-to-M channel-sounding experimental campaign and the signal processing techniques used to process the collected data.

A. Measurement Campaign Description

The MIMO M-to-M channel-sounding experimental campaign was conducted along the surface streets near Georgia Tech campus, in the midtown Atlanta metropolitan area. Major test assets associated with the campaign were two Econoline vans equipped with a power generator and rechargeable power supplies. Each van was equipped with a linear antenna array, consisting of four vertically-polarized, magnetic-mount, 2.435 GHz antenna elements. The antenna elements were placed across the roof of the van from the passenger side of the van to the driver side of the van and spaced 2.943 wavelengths apart from each other. The vans were usually driven in a convoy fashion (in the same lane and at the same speed), roughly 100 m to 300 m apart, and with speeds up to 60 mph.

Fig. 2 (a) depicts the block diagram for the MIMO transmitter system, located in the trailing vehicle. A rubidium clock provided a common 10 MHz reference for two Agilent E4438C signal generators. The third generator, an Agilent E4433B, synchronized the two E4438C signal generators. The arbitrary waveform feature of the E4438C signal generators was used to program orthogonal OFDM channel sounding waveforms to support 2×4 MIMO channel matrix estimation. One source transmitted on the odd subcarriers, while the other source transmitted on the even subcarriers. An FFT size of $N = 256$ was used for the OFDM signal with a sample rate of 32 million complex samples per second. The OFDM symbols were transmitted in a loop-back fashion with a pulse repetition interval of 300 μs, which corresponds to a maximum resolvable Doppler shift of 3.3 kHz. The signal generator output signals were passed through linear amplifiers and then coupled to two adjacent antenna elements in the antenna array.

Fig. 2 (b) shows the block diagram for the MIMO receiver system, located in the leading vehicle. The signals were received by a four-element linear antenna array. Each of the received signals was coupled to a low-noise amplifier with 20 dB gain. The signals were then passed to VME-based radio frequency (RF)-to-intermediate frequency (IF) signal down-converters from Mercury Computer Systems, which converts the RF analog signal to an IF frequency of 20 MHz. The resulting analog signals were sent pairwise into Pentek model 6235 wide-band receiver boards that performed anti-aliasing

filtering, analog-to-digital conversion at a 72 MHz complex sample rate, digital down-conversion of the signals to complex baseband, and the 4:1 decimation and filtering. The wideband receiver was clocked with an Agilent E4433B source with a 10 MHz reference from a rubidium clock source. The channels were synchronized pairwise. The use of the rubidium sources in the both vans provided a mechanism to achieve frequency synchronization between the transmit and receive subsystems. The resulting baseband samples of each pairwise set from the digital down-converters were multiplexed and stored temporarily in a 2 GByte buffer, and were then streamed to a computer and stored on a hard disk. The buffer boards enabled 3 s contiguous snapshots to be collected from each of the 4 simultaneous channels at the sample rates of 32 million complex samples per channel per second. Due to processing memory constraints, the samples associated with any one snapshot were partitioned into eighteen time-contiguous segments. Snapshots were collected roughly 30 s apart.

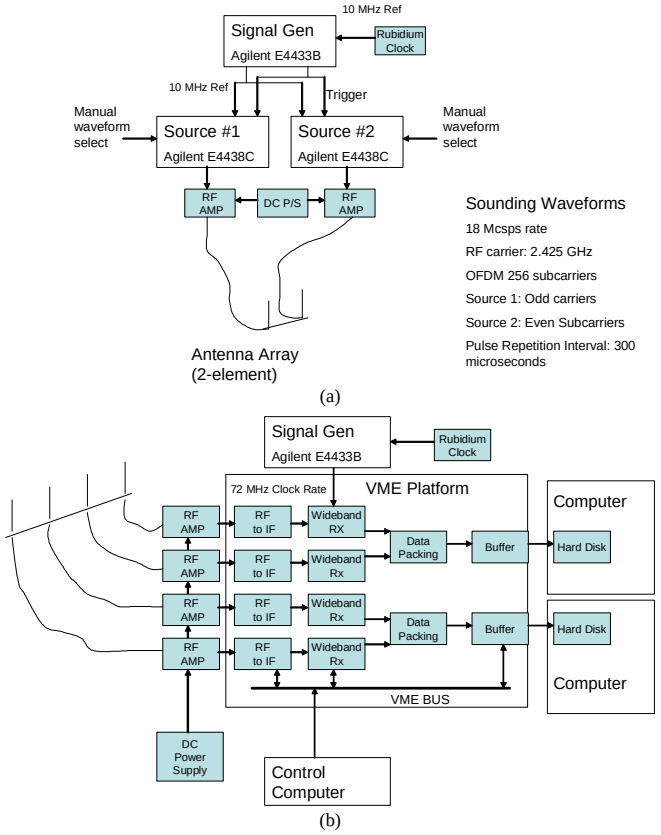

Fig. 2. The block diagram of the MIMO transmitter system (a) and the block diagram of the MIMO receiver system (b).

Channel sounding waveforms were transmitted from the trailing vehicle and the signals were received and recorded by the leading vehicle. Video cameras were used in the vehicles to provide indications of time, velocity, and location, to support post-test processing of the collected data. The measurements typically included both LoS and NLoS conditions, as other vehicles and obstructions often masked the direct LoS. Details associated with the measurement campaign are summarized in Table II. Finally, Fig. 3 shows photograph of the location where the data used in the paper were collected.

TABLE II
DESCRIPTION OF THE MEASUREMENT CAMPAIGN.

Carrier Frequency	2.435 GHz
Tx Antenna Configuration	2.4 GHz magnetic mount antennas mounted in a 1x4 linear array on the van rooftop; 2 adjacent elements from the array were used for transmission
Rx Antenna Configuration	2.4 GHz magnetic mount antennas mounted in a 1x4 linear array on the van rooftop
Signal Modulation	OFDM symbols with 256 subcarriers
Transmit Sample Rate (used to generate the OFDM signal)	36 MHz
Transmit Waveform pulse repetition interval	The pulse repetition interval of the sounding waveform was approximately 300 microseconds
Frequency Synchronization	Rubidium clocks at the transmitter and the receiver
Data collection System	Pentek-based VME custom collection system with Mercury Computer Systems RF front ends; 4-channel receiver with pairwise sample synchronization
Data collection products at the receiver per snapshot (corresponding roughly to 3-second durations of contiguous data)	Approximately 55M contiguous complex baseband samples per antenna output
Collection Scenario with mobile vans	Vans traveling 25 to 45 mph in the same direction and within 100 m to 300m apart in an urban area around Georgia Tech.

Fig. 3. Photograph of the street around Georgia Tech campus where the channel-sounding experimental campaign was conducted.

B. Data Processing

Our wideband channel model is focused on characterizing the fast-fading characteristics of the channel. To allow fair comparison between our wideband channel model and the measured data, the slow-fading component of the measured signal envelope is removed. This is achieved using the local sliding window technique [18], where the sliding window length is set to 20λ. Furthermore, to allow comparison between the theoretical normalized space-time-frequency correlation function (STF-CF) in [10] and the STF-CF obtained from measured data, the power of each measured subchannel $A_T^{(p)}$ - $A_R^{(q)}$ is normalized to unity. This normalization is performed

as follows:

$$\hat{h}_{pq}(n\Delta t_s, k\Delta\tau_s) = \frac{h_{pq}(n\Delta t_s, k\Delta\tau_s) - \hat{m}_{pq}(k\Delta\tau_s)}{\hat{\sigma}_{pq}(k\Delta\tau_s)}, \quad (12)$$

where $h_{pq}(n\Delta t_s, k\Delta\tau_s)$ is the measured input delay-spread function, $n \in \{0, \ldots, N_t - 1\}$, $k \in \{0, \ldots, N_\tau - 1\}$, Δt_s and N_t denote the sampling period and the number of samples with respect to the time variable t, $\Delta\tau_s$ and N_τ denote the sampling period and the number of samples with respect to the delay variable τ, and $\hat{m}_{pq}(k\Delta\tau_s)$ and $\hat{\sigma}^2_{pq}(k\Delta\tau_s)$ are the estimated mean and variance of the measured $A_T^{(p)}$ - $A_R^{(q)}$ subchannel, respectively. The estimated mean and variance are calculated as $\hat{m}_{pq}(k\Delta\tau_s) = N_t^{-1}\sum_{n=0}^{N_t-1} h_{pq}(n\Delta t_s, k\Delta\tau_s)$ and $\hat{\sigma}^2_{pq}(k\Delta\tau_s) = N_t^{-1}\sum_{n=0}^{N_t-1} |h_{pq}(n\Delta t_s, k\Delta\tau_s) - \hat{m}_{pq}(k\Delta\tau_s)|^2$.

From the normalized input delay-spread function $\hat{h}_{pq}(n\Delta t_s, k\Delta\tau_s)$, we can calculate the STF-CF, the sD-psd, the psds, and the LCR. The STF-CF is obtained as follows:

$$\hat{R}_{pq,\tilde{p}\tilde{q}}(T\Delta t_s, F\Delta f_s) = (N_t N_\tau)^{-1} \sum_{n=0}^{N_t-1}\sum_{k=0}^{N_\tau-1} \hat{T}_{pq}(n\Delta t_s, k\Delta f_s)^* \hat{T}_{\tilde{p}\tilde{q}}((n+T)\Delta t_s, (k+F)\Delta f_s), \quad (13)$$

where $T \in \{0, \ldots, t_{\max} - 1\}$, $F \in \{0, \ldots, f_{\max} - 1\}$, $t_{\max} = \lceil 1/(\Delta t_s f_D)\rceil$, $f_{\max} = \lceil 1/(\Delta f_s \tau_{\max})\rceil$, f_D is the maximum Doppler frequency, and $\tau_{\max}$ is the maximum relative delay.[1] The normalized time-variant transfer function $\hat{T}_{pq}(n\Delta t_s, k\Delta f_s)$ is obtained from the normalized input delay-spread function $\hat{h}_{pq}(n\Delta t_s, k\Delta\tau_s)$ using a fast Fourier transform. The space-Doppler power spectral density is obtained using the Welch algorithm [19]. The psds is obtained by averaging the squared magnitudes of the normalized input delay-spread function $\hat{h}_{pq}(n\Delta t_s, k\Delta\tau_s)$ over all times $n\Delta t_s$. Finally, the LCR, $L(R)$, is obtained by counting how many times per second the measured signal envelope crosses the level R in the positive going direction.

IV. Reference Model Validation

In this section, we compare the sD-psd, the psds, and the LCR obtained from the reference model with those obtained from the measurement campaign described in Section III. The expressions for the theoretical sD-psd, psds, and LCR are derived in [10] and [11]. The wideband channel measurements collected in the urban surface street area (shown in Fig. 3) were performed at 2.435 GHz and the maximum Doppler frequencies were $f_{T\max} = f_{R\max} = 90.86$ Hz. The distance between the $\mathrm{T_x}$ and $\mathrm{R_x}$ was approximately $D = 300$ m and the moving directions were $\gamma_T = \gamma_R = 90°$. Both, the $\mathrm{T_x}$ and $\mathrm{R_x}$ were equipped with two omnidirectional antenna elements with the azimuth and elevation angles $\theta_T = \theta_R = 0°$ and $\psi_T = \psi_R = 0°$, respectively. All antenna elements have the same height, $\Delta_H = 0$, and the distance between the antenna elements is $d_T = d_R = 2.943\ \lambda$. It is assumed that the path loss exponent γ is 4, which is typical for radio propagation over a flat reflecting surface [21].

[1]Operation $\lceil\cdot\rceil$ denotes rounding up to the next integer.

The analytical STF-CF is obtained by assuming that the number of local scatterers around the $\mathrm{T_x}$ and $\mathrm{R_x}$ is very large. According to the Central Limit Theorem, this assumption is valid if each input delay-spread function $h_{pq}(t, \tau)$ has a complex Gaussian distribution. Before we can compare the theoretical and measured data, we need to confirm that the measured input delay-spread functions have complex Gaussian distributions. Fig. 4 shows that the pdf of the real and imaginary components of the measured (normalized) input delay-spread function, $\hat{h}_{11}(t, \tau)$, can be closely approximated by a Gaussian distribution. Furthermore, the pdf of the measured amplitude and phase can be closely approximated by a Rice and uniform distribution[2], respectively. Similar results were observed for all the measured input delay-spread functions.

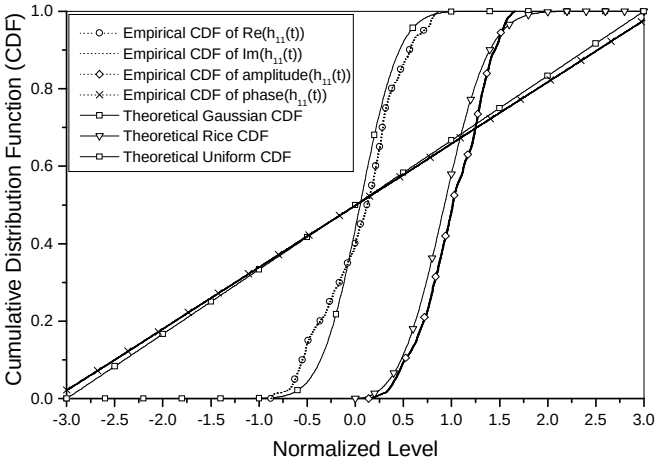

Fig. 4. Theoretical and empirical distribution functions of $h_{11}(t, \tau)$ in an urban surface street area.

Figs. 5 - 7 compare the analytical and the measured sD-psd, psds, and LCR for the urban surface street environment, respectively. The analytical curves are obtained with the parameters $\beta_{Tm} = 5.1°$, $\beta_{Rm} = 10.2°$, $\mu_T = 73.3°$, $\mu_R = 264.7°$, $k_T = 5.7$, $k_R = 6.4$, $\eta_T = 0.043$, $\eta_R = 0.137$, $\eta_{TR} = 0.82$, $R_{t1} = R_{r1} = 9.6$ m, $R_{t2} = R_{r2} = 96$ m, and $K = 2.41$. These parameters are estimated using the method proposed in [13]. The parameters γ, D, γ_T, γ_R, θ_T, θ_R, ψ_T, ψ_R, d_T, d_R, Δ_H, $f_{T\max}$, and $f_{R\max}$ are selected to match the measurement conditions as described above.

Figs. 5 - 7 show close agreement between the theoretical and empirical curves. These results confirm the utility of the proposed model and show that double-bounced rays bear more energy than the single-bounced rays in urban surface street environments.

V. Conclusions

This paper reviewed our 3-D reference model for wideband MIMO M-to-M channels. To validate this model, a MIMO M-to-M channel-sounding experimental campaign was conducted in the Atlanta metropolitan area. The measured data was processed and compared with the analytical predictions. The

[2]With non-isotropic scattering, the phase may not be uniform distributed.

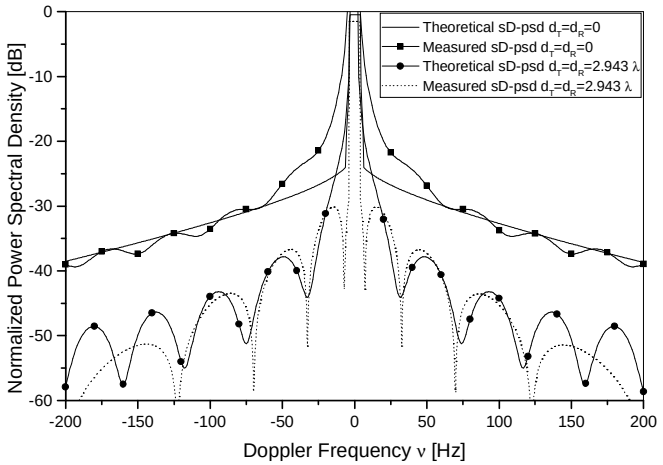

Fig. 5. The theoretical and the measured sD-psd in an urban surface street area.

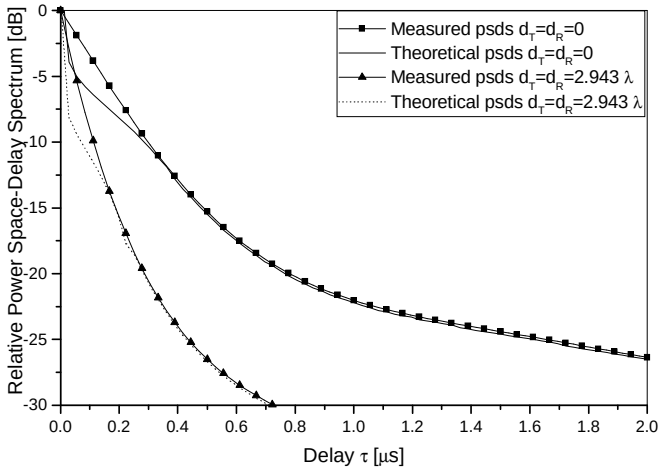

Fig. 6. The theoretical and the measured psds in an urban surface street area.

close agreement between the analytical and empirical curves confirms the utility of the proposed reference model.

DISCLAIMER

The views and conclusions contained in this document are those of the authors and should not be interpreted as representing the official policies, either expressed or implied, of the Army Research Laboratory or the U. S. Government.

REFERENCES

[1] A. S. Akki and F. Haber, "A statistical model for mobile-to-mobile land communication channel," *IEEE Trans. on Veh. Tech.*, vol. 35, pp. 2–10, Feb. 1986.

[2] R. Wang and D. Cox, "Channel modeling for ad hoc mobile wireless networks," *Proc. IEEE VTC*, pp. 21–25, Birmingham, AL, May 2002.

[3] C.S. Patel, G.L. Stüber, and T. G. Pratt, "Simulation of Rayleigh-faded mobile-to-mobile communication channels," *IEEE Trans. on Commun.*, vol. 53, pp. 1876–1884, Nov. 2005.

[4] A.G. Zajić and G.L. Stüber, "A new simulation model for mobile-to-mobile Rayleigh fading channels," *Proc. IEEE WCNC*, pp. 1266–1270, Las Vegas, NE, USA, Apr. 2006.

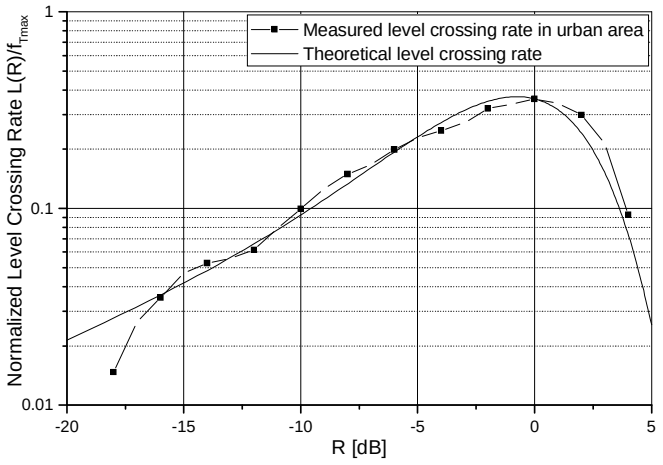

Fig. 7. The theoretical and the measured LCR in an urban surface street area.

[5] J. Maurer, T. Fügen, and W. Wiesbeck, "Narrow-band measurement and analysis of the inter-vehicle transmission channel at 5.2 GHz,"*Proc. IEEE VTC*, pp. 1274–1278, Birmingham, AL, USA, May 2002.

[6] G. Acosta, K. Tokuda, and M. A. Ingram, "Measured joint Doppler-delay power profiles for vehicle-to-vehicle communications at 2.4 GHz," *Proc. IEEE GLOBECOM*, pp. 3813–3817, Dallas, TX, USA, Nov. 2004.

[7] M. Pätzold, B.O. Hogstad, N. Youssef, and D. Kim, "A MIMO mobile-to-mobile channel model: Part I-the reference model," *Proc. IEEE PIMRC*, pp. 573–578, Berlin, Germany, Sept. 2005.

[8] A.G. Zajić and G.L. Stüber, "Space-time correlated MIMO mobile-to-mobile channels," *Proc. IEEE PIMRC*, Helsinki, Finland, Sept. 2006.

[9] A.G. Zajić and G.L. Stüber, "A three-dimensional MIMO mobile-to-mobile channel model," *IEEE WCNC*, Hong Kong, Mar. 2007.

[10] A.G. Zajić and G.L. Stüber, "A three dimensional parametric model for wideband MIMO mobile-to-mobile channels," to appear in *Proc. IEEE GLOBECOM*, Washington, D.C., USA, Nov. 2007.

[11] A.G. Zajić, G.L. Stüber, Thomas G. Pratt, and Son Nguyen, "Envelope level crossing rate and average fade duration in mobile-to-mobile fading channels," to appear in *Proc. IEEE ICC*, Beijing, China, May 2008.

[12] A.G. Zajić and G.L. Stüber, "A 3-D simulation models for wideband MIMO mobile-to-mobile channels," *Proc. IEEE MILCOM*, Orlando, FL, USA, Oct. 2007.

[13] A.G. Zajić, G.L. Stüber, Thomas G. Pratt, and Son Nguyen, "Wideband MIMO mobile-to-mobile channels: statistical modeling with experimental verification," submitted to *Proc. IEEE Trans. on Veh. Tech*,, Jan. 2008.

[14] D. Gesbert, H. Bölcskei, D.A. Gore, and A.J. Paulraj, "Outdoor MIMO wireless channels: models and performance prediction," *IEEE Trans. on Commun.*, vol. 50, pp. 1926–1934, Dec. 2002.

[15] A. Abdi, J. A. Barger, and M. Kaveh, "A parametric model for the distribution of the angle of arrival and the associated correlation function and power spectrum at the mobile station," *IEEE Trans. on Veh. Tech.*, vol. 51, pp. 425–434, May 2002.

[16] J.D. Parsons and A.M.D. Turkmani, "Characterisation of mobile radio signals: model description," *IEE Proc. I, Commun., Speach, and Vision*, vol. 138, pp. 549–556, Dec. 1991.

[17] A. Kuchar, J.-P. Rossi, and E. Bonek, "Directional macro-cell channel characterization from urban measurements," *IEEE Trans. on Antennas and Propagation*, vol. 48, pp. 137–146, Feb. 2000.

[18] W. C. Y. Lee,"Estimate of local average power of mobile radio signal," *IEEE Trans. on Veh. Tech.*, vol. 34, pp. 22–27, Feb. 1985.

[19] P. D. Welch, "The use of fast fourier transform for the estimation of power spectra: a method based on time averaging over short, modified periodograms," *IEEE Trans. Audio Electroacoustics*, vol. AU-15, pp. 70–73, June 1967.

[20] L. J. Greenstein, D. G. Michelson, and V. Erceg, "Moment-method estimation of the Ricean K-factor," *IEEE Commun. Letters*, vol. 3, pp. 175–176, June 1999.

[21] G. L. Stüber, *Principles of mobile communication 2e.*Kluwer, 2001.